Submitted to ADVANCED MATERIALS

DOI: 10.1002/adma.((please add manuscript number))

On-demand patterning of nano-structured pentacene transistors by scanning thermal lithography

By *Joseph E. Shaw, Paul N. Stavrinou* and *Thomas D. Anthopoulos**

[*] Prof. T. D. Anthopoulos, Dr. P. Stavrinou and Mr J. E. Shaw
Centre for Plastic Electronics and Department of Physics
Blackett Laboratory, Imperial College London, SW7 2AZ (UK)
E-mail: t.anthopoulos@ic.ac.uk

Keywords: Organic semiconductors, pentacene transistors, nanolithography, scanning thermal lithography, thermochemical lithography, scanning lithography

Developments in the emerging class of organic semiconductors are continuing at pace and in many instances are now widely seen to offer a genuine alternative, along with attendant benefits, to traditional inorganic-based technologies. Organic semiconductors present a number of attractions one of which is the relatively simple chemistry that offers highly tunable electro-optical properties allied with the potential for inexpensive, solution-based manufacturing processes. The low temperature processability of organics also makes them compatible with low-cost substrate materials such as plastic; rendering them suitable for application in the burgeoning area of plastic electronics. Despite the excellent progress, however, an important challenge for the wider deployment of the technology is the inability to pattern organic materials with high resolution. It is fair to say that in comparison to what is achieved with inorganic materials, delivering sub-micron patterning with organics has remained some way behind. This technological bottleneck has thus far limited the application of organics to large-area opto/electronics such as photovoltaic cells, light-emitting diodes and thin-film transistor (TFTs) backplanes for flat panel display (1).

Organic based devices comprising sub-micron elements are important because they could seed future developments in the field of nanoelectronics as well as enable advanced studies into

the fundamental opto/electronic processes in organic materials at the nanoscale. Furthermore, the availability of organic-compatible nano-patterning methods could potentially allow the fabrication of organic-based sensors(2-4) on a scale not previously achieved. The latter could significantly improve their speed and sensitivity and hence pave the way for future developments.

A promising area of research attempting to address the issue of nano-manufacturing is the manipulation and patterning of materials using direct scanning probe tools. Methods demonstrated to date include; AFM ploughing (5), dip-pen nanolithography and dip-pen stamp-tip(6), application of electrical current through a conducting tip(7), scanning near-field optical microscopy(8) and the subject of the present paper, the use of heatable AFM probes to initiate chemical reactions in carefully designed materials. Scanning probe methods can be successfully used to produce features down to the same size as the tip width or even smaller.(9) The thermochemical conversion of materials induced by a heated AFM probe [**Figure 1(a)**] is a relatively recent innovation, with much of the pioneering work performed by Mamin *et al.* (10, 11) and King *et al.* (12-14). Perceived uses of this technique include local surface energy modification and high density data storage (15) and production of nano-circuitry. Recent work of note involves the reduction of the insulating graphene oxide to ~30 nm wide conductive graphene nanoribbons (16), the production of ferro-electric nanostructures (17), the thermal conversion of a polyphenylene vinylene precursor to a conjugated polymer (9) as well as the studies by Vancso et al., on fundamental heat transport (18-20). The versatility and precision of this method is so great that it has even been used to produce 3D structures of molecular photoresist and write features with resolutions below 30 nm at speeds approaching that of electron beam lithography (21). Despite the enormous potential of the method, including work and patent applications which cover the use of scanning thermal lithography to pattern resists or other materials for the aim of producing functional nanostructures(22), active nanoscale device fabrication has yet to be demonstrated using either organic or inorganic materials.

Here, we demonstrate that scanning thermal lithography can be used to chemically convert a soluble pentacene precursor into semiconducting pentacene nanostructures with extremely high spatial resolution on arbitrary substrates including SiO_2, glass and plastic. Well-defined semiconducting pentacene nanoribbons were produced on-demand with widths down to 73 nm and up to 90 μm in length with remarkably high yield. Our study also highlights how the scanning direction and speed of the heated tip may all be used to control the growth and orientation of the pentacene crystalline domains comprising the individual nanoribbon-like structures. To demonstrate unambiguously the semiconducting nature of these on-demand patterned 1-dimensional (1D) nanoribbon-like pentacene nanostructures, we have produced field-effect transistors composed of varying numbers of pentacene nanoribbons. As-prepared transistors show p-channel behaviour with hole mobilities comparable to values obtained from micron-scale devices prepared using conventional hotplate annealing. The present study demonstrates real progress towards producing functional on-demand patterned nanoscale organic electronics and establishes how scanning thermal lithography could enable the realisation of more complex nanoscale devices.

The pentacene precursor 13,6-*N*-Sulfinylacetamidopentacene [**Figure 1(b)**] was dissolved in chloroform and spin cast directly onto Si^{++}/SiO_2 substrates at room temperature to form a 20 nm (±5 nm) thick film. As-spun precursor films are found to be amorphous and highly uniform. **Figure 1(c)** displays a representative as-measured AFM topography image of the precursor film before conversion. Heating on a hot plate for 1 min at 200 °C(23) the precursor films convert into pentacene as indicated by the formation of extended micron-size crystalline domains [**Figure 1(d)**]. The crystalline nature of these pentacene domains has been verified by polarized light optical microscopy measurements [e.g. appearance of strong birefringence shown in **Figure S2**, Supplementary Information (SI)]. These large poly-crystalline domains are surrounded by smaller domains with diameters down to ~100 nm. To investigate whether similar

conversion behaviour can be observed in films treated using the scanning thermal lithography, we scanned small areas of the precursor film (2×2 μm) with the heated AFM tip (500 ℃) in contact mode [**Figure 1(e)**]. We note that **Figure 1** display the as-measured AFM images since tip deconvolution processing algorithms was found to have little or no effect on the final topography image (see SI section).

The scanned areas revealed a decrease in film thickness, consistent with the anticipated mass loss in the precursor conversion to pentacene. The average pentacene domain size was generally much smaller with a more uniform size distribution compared to hot-plate converted pentacene films. This difference was attributed to the smaller surface area of the heated tip serving to confine the crystal growth to nanometres size domains. It is also noteworthy that the precursor film is subjected to a rapid period of heating from the heated tip travelling at speeds of several μm/s in comparison to the slow pentacene growth allowed by the uniform heating on a hot plate. A consequence of the variation of heated probe parameters is the direct effect on the growth dynamics and orientation of the crystalline pentacene domains.

Using a fixed tip temperature of 500℃ we obtained randomly oriented pentacene domains of dimensions which vary with scan speed. **Figure 2(a-b)** shows the effect of scanning speed on the resulting film morphology for a tip temperature of 500℃. Low speed scans (2 μm/s) result in the formation of larger pentacene crystalline domains [**Figure 2(a)**] while faster scans (16 μm/s) typically yield smaller domains [**Figure 2(b)**]. The effect of scan speed on converted pentacene domains is better illustrated in **Figure 2(c-e)** where the statistical distribution of the average domain size is shown for three different scan speeds. Further increase in the scanning speed sees the average domain width decreasing and approaching the width of the tip (70-100 nm).

On increasing the contact force between the tip and the precursor film, deep furrows could be ploughed into the surface of the film. The width of each furrow was approximately 70-100 nm and found to be relatively independent of tip speed and film thickness. Within these furrows we observed the formation of highly oriented pentacene crystalline domains along the scan direction [**Figure 3(a)**]. The pentacene domains produced had varying lengths (*d*) [**Figure 3(b)**] while the widths (*w*) were roughly confined to the width of the probe furrows (60-100 nm). On increasing the speed [8 μm/s in **Figures 3(c)** and **(d)**, and 16 μm/s in **(e)** and **(f)**] the domain length was found to decrease, whilst still retaining the same width. Upon a further increase of the scan speed a point was reached where the pentacene precursor didn't convert to pentacene and only parallel lines of precursor film were present. The depth at which conversion of the precursor molecule to pentacene occurs could also be modulated by carefully controlling the scan speed for a fixed film thickness. **Figure 3(g)** shows the cross-section of an AFM image of four parallel lines written at four different tip speeds (10, 5, 1 and 0.1 μm/s), at a fixed tip temperature, revealing the presence of successively deeper furrows for slower scan speeds. This is attributed to increased conversion of precursor, and the associated mass-loss, for slower scans. These results demonstrate the ability to control the conversion reaction across the precursor film with excellent accuracy.

Further work was carried out to produce stand-alone pentacene nanostructures with well-defined size and shape using the scanning thermal lithography. Scans were confined to single-pass lines and used to produce pseudo 1D pentacene nanoribbons. As already highlighted, the thickness of nanowire features depends on the amount of heat transferred and on the thickness of the precursor film(9). According to finite element simulations and experimental work(24), for increasingly lower temperatures when the film thickness falls below that of the diameter of the heated probe, the transfer of heat becomes increasingly vertical and reaches a natural limit of the width of the tip. To test this hypothesis, precursor films with thicknesses similar to that used for

producing micron-scale thin-film transistors (20 (±5) nm), were used. A fixed tip temperature of 500 ℃ and scan speeds below 1 μm/s produced features with widths >1 μm; on increasing the scan speed to 25 μm/s the minimum feature width decreases to ~70-100 nm. Thus in the case of our 20 nm thick precursor film and 70-100 nm tip width, the vertical heat transfer model appears to hold true. Beyond this speed limit, the nanoribbons' width remains approximately the same, but the structures became increasingly intermittent. A detailed discussion of factors affecting the conversion of precursor and the resolution of features can be found in the SI section.

A further important advantage of the scanning thermal lithography is the ability to design and pattern arbitrary shapes of thermo-chemically converted pentacene nanoribbons. **Figure 4(a)** shows a micron-size logo of the Centre for Plastic Electronics (CPE) at Imperial College London, written by this method onto a plastic (PET) substrate. The same approach was used for direct patterning of isolated pentacene nanoribbons onto conductive electrodes. **Figure 4(b)** shows an AFM topography image of two pentacene nanoribbons (written at 25 μm/s) patterned over and across a pair of gold source-drain electrodes. Dipping the as patterned transistor structures into a bath of methanol was found to dissolve and remove the unconverted pentacene precursor leaving behind the pair of stand-alone pentacene nanoribbons. **Figures 4(c)** and **(d)** show a representative AFM topography image and the corresponding cross section of such nanostructure revealing the thickness (~17 nm) and width (~73 nm) and width of the developed nanoribbon.

The ability to create standalone organic nanostructures with controlled texture is an extremely useful property as it allows, firstly, the sequential deposition and conversion of different precursor materials with extraordinary simplicity, and secondly, the rapid prototyping of nanoscale devices and potentially integrated nano-circuits. Such on-demand patterned 1D structures could also be used to study the structure-property relationship in organic semiconductors with unprecedented accuracy. To this end, the vast majority of fundamental

studies reported to date have been confined to thin films. Malliaras *et al.*, for example, has reported extensively on factors that affect growth of vacuum sublimed pentacene films and the impact on their electronic properties(25, 26). However, to date there has been no report on hole transport across well-defined nanostructured grain boundaries or across devices based on 1D pentacene nanowires.

In order to quantify the hole transport across the pentacene nanoribbons, we fabricated tens of bottom-gate, bottom-contact pentacene nanoribbon based transistors. The device architecture used is schematically depicted in **Figure 5(a)**. Here, scanning thermal lithography was used to produce, in ambient air, block shaped hole-transporting channels comprising a large as well as a small number of individual pentacene nanoribbons [**Figure 5(b-c)**]. **Figure 5(d)** displays a typical set of transfer characteristics recorded for a pentacene transistor fabricated by scanning thermal lithography in air. The channel length of the device is 2.5 μm while the width is composed of approximately 70 parallel (70-100 nm wide) pentacene nanoribbons yielding a total channel width of ~7-8 μm. The device performance was found to be very uniform, with all transistors yielding hole mobilities in the range 10^{-5}-10^{-4} $cm^2V^{-1}s^{-1}$. Similar values have been obtained from control experiments where conventional large-area transistors were fabricated using films of the same pentacene precursor annealed at 150 ℃ in air using a hotplate. The relatively low mobility, as compared to previously reported values for the same precursor(27, 28), is believed to be due to the quality of the precursor material used and possibly to the non-optimised transistor architecture used (e.g. bottom-gate, coplanar transistor architecture).

A further interesting observation is the highly anisotropic hole transport characteristics observed between transistors based on pentacene nanoribbons patterned perpendicular (⊥) and parallel (∥) to the source-drain electrodes. Optimum performance was obtained from transistors comprising pentacene nanoribbons patterned perpendicular to the metal electrodes while no hole

transport/accumulation could be observed in devices based on nanoribbons patterned parallel to the electrodes. This is attributed to the stand-alone nature of the pentacene nanoribbons. Supporting evidence of this is shown in **Figure 5(e)** where analysis of the high resolution AFM image reveals the appearance of closely packed standalone pentacene nanoribbons separated by very narrow air gaps 5-15 nm wide.

These measurements not only show how one could use a scanning heated tip to produce pentacene nanoribbons but also how these structures can be tuned so that electrical conduction across them is strictly dominated by intra-ribbon rather than inter-ribbon hole transport. The unique ability to accurately manipulate the texture and electronic properties of the pentacene nanoribbons is further illustrated in **Figure 5(f)** where the hole mobility is plotted as a function of tip scan speed for a set of transistors with fixed channel length (L = 10 μm) and varying width (W = 20 μm or 40 μm). At tip speeds of 4 μm/s, or below, the hole mobility is zero due to the high tip temperature (500 °C) under which the material tends to decompose and/or sublime (formation of holes). For scanning speeds >32 μm/s, a similar mobility decrease is observed but in this case it is attributed to the incomplete conversion of the precursor to pentacene. The latter is further verified by the ease with which these not fully converted structures can be washed away once the substrates are immersed into a solvent bath. Only for optimised writing speeds of 12-20 μm/s, a clear formation of well-defined stand-alone pentacene nanoribbons can be observed.

Lastly, on comparing the size of pentacene crystalline domains produced by scanning thermal lithography with those produced by the hot plate, we found the average size of the pentacene domain was far larger for the hot-plate annealed films; the latter method resulted in films comprising larger crystalline domains interspersed among much smaller crystals 100-300 nm in size. This is in contrast to the, relatively, uniform size of pentacene crystalline domains

(100-200 nm) produced by the heated tip. Rationalising these observations, we argue that hole transport in both types of devices appears to be limited by the smallest size pentacene crystals. The similarity in the size of these small crystalline domains could be one reason why both hot-plate annealing and scanning thermal lithography yield pentacene transistors with comparable hole mobilities.

To summarise, we have successfully demonstrated direct patterning of semiconducting pentacene nanoribbon-like structures on arbitrary substrates and their integration in active nanoscale organic transistors using an electrically heated AFM cantilever. Semiconductor patterning and device fabrication was performed in air without any special precautions using a conventional AFM system and a commercially available solution-processable pentacene precursor. The extraordinary simplicity and the maskless on-demand nature of the method coupled with the rapidity with which the active devices can be produced, makes scanning thermal lithography an ideal tool for the rapid prototyping of active nanostructured electronics based not only organic precursors but also on inorganic systems such as solution processable metal oxide precursors(17).

Experimental

Materials and film preparation: 13,6-*N*-Sulfinylacetamidopentacene(27) was obtained from Sigma-Aldrich and used as received. Chloroform and chlorobenzene were the two main solvents used in this study. Precursor solutions based on chlorobenzene were found to be stable when used under nitrogen ambient but degraded upon contact with air after several hours. Chloroform solution on the other hand was found to produce precursor films that remained stable for several days even when stored in air. All precursor films studied here were processed by spin casting a freshly prepared 20 mg/ml chloroform solution at 1500 rpm under nitrogen. Freshly

prepared samples were then transferred to the AFM Agilent 5500 system integrated with an Anasys Instruments NanoTA thermal AFM tip system for performing the scanning lithography. Conventional thermal annealing was performed in air using a standard IKA hotplate.

Transistor fabrication: Bottom-gate, bottom contact transistors structures were fabricated using heavily doped p-type Si wafers acting as a common gate electrode and a 200 nm thermally grown SiO_2 layer as the dielectric. Using conventional photolithography, gold source-drain (S-D) electrodes were defined with channel lengths and widths in the range 1-40 μm and 1-20 mm, respectively. A 10 nm layer of titanium was used as an adhesion layer for the gold on SiO_2. The finished electrodes were 100 nm thick. The SiO_2 surface was passivated with hexamethyldisilazane (HMDS) purchased from Aldrich. The latter is often used to modify the SiO_2 surface and contact angle to improve organic transistor characteristics. Devices fabricated on untreated SiO_2 showed no transistor function. The chloroform precursor solution was finally spin coated onto 1.5 cm × 1.5 cm size substrates containing few hundreds of prepatterned S-D electrode pairs at 1500 rpm. The resulting precursor film thickness was ~20 nm. Scanning thermal lithography was then performed in air through multiple scans of the heated tip between the S-D electrodes. Scanning was performed either in parallel or perpendicular to the gold electrodes but functioning transistors were achieved only in the case where the scanning thermal lithography was performed in a direction perpendicular to the electrodes. The heat transfer theory used in this work is reported in the SI section and was adopted from Fenwick *et al.* (9) and Wei *et al.* (16).

Transistor characterisation: The transistor current-voltage characteristics were obtained in a micro-probe station with a high-precision Keithley 4200 semiconductor parameter analyser. All measurements were obtained in ambient air. The relative air humidity during testing was in the range 40-60%. Charge carrier mobility was calculated using the standard gradual channel approximation model (29).

Acknowledgements

We acknowledge financial support from the European Research Council (ERC) and Engineering and Physical Sciences Research Council (EPSRC).

Received: ((will be filled in by the editorial staff))
Revised: ((will be filled in by the editorial staff))
Published online: ((will be filled in by the editorial staff))

Figures

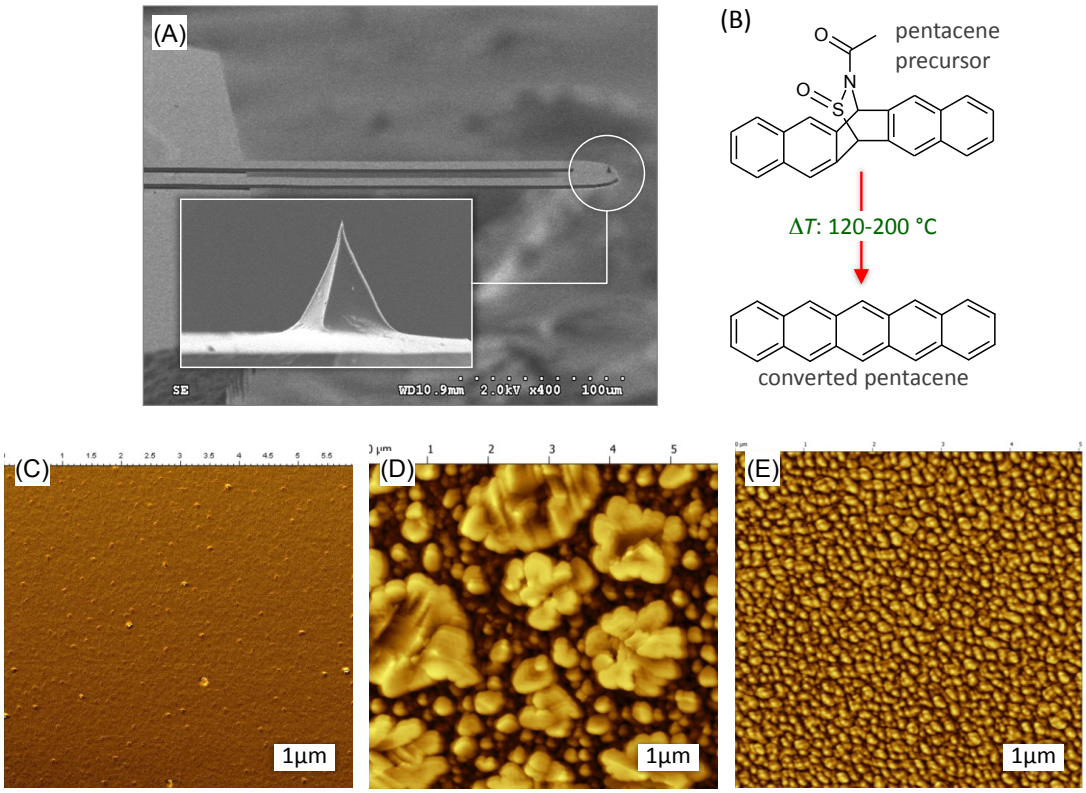

Figure 1. (A) Scanning electron microscope (SEM) images of an Anasys AN 2-200 Thermalever resistive heater silicon probe and a close-up of its tip [Image: Anasys Instruments]. The probe is mounted on a proprietary dual-contact cantilever holder and heated up to 500 ℃. (B) Molecular structures of the pentacene precursor 13,6-N-Sulfinylacetamidopentacene and pentacene upon thermal conversion at temperatures between 120-200 ℃. (C)-(E) AFM topographical images of pentacene precursor and converted pentacene films. (C) 13,6-N-Sulfinylacetamidopentacene film spincoated from a chloroform solution onto a Si^{++}/SiO_2 substrate. (D) Pentacene converted using a hot-plate at 200 ℃ for 1 minute in air. The resulting pentacene film contains large crystalline domains randomly interspersed among smaller crystalline domains with sizes down to 100 nm. (E) Pentacene film converted by scanning thermal lithography using the heated silicon tip (500 ℃) and a scanning speed of 3 µm/s.

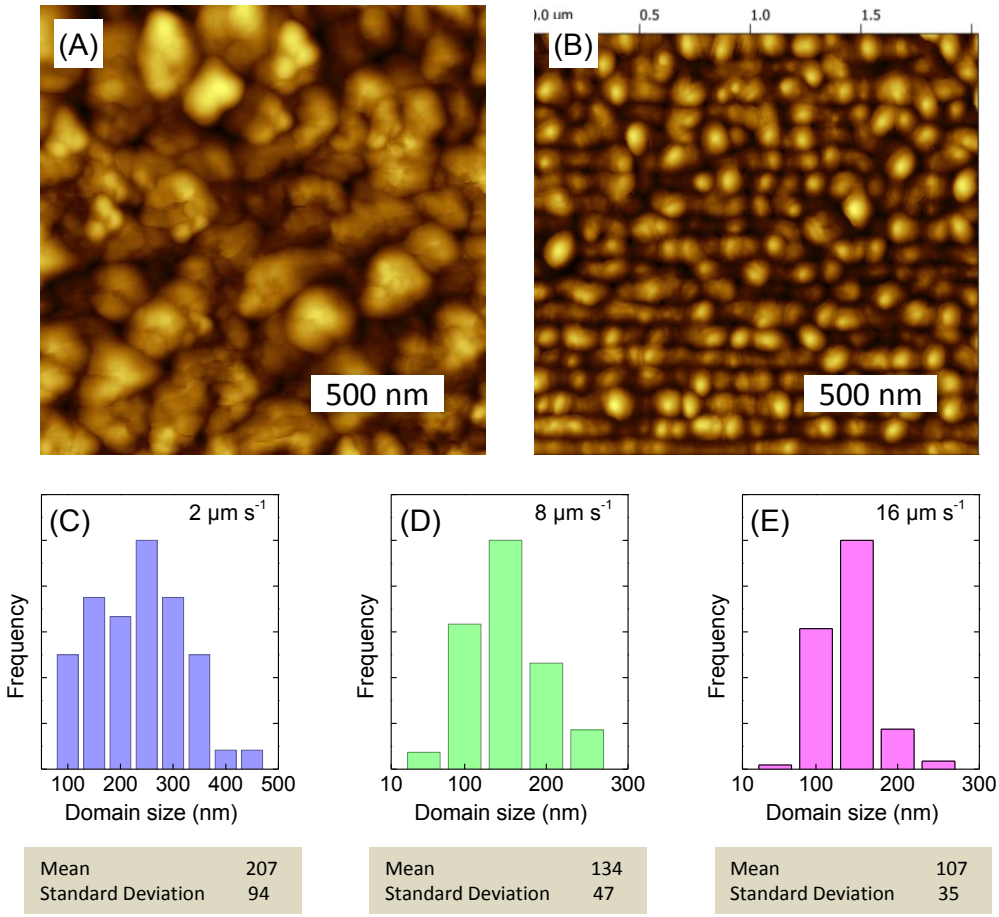

Figure 2. AFM topographical images of pentacene films converted by the scanning heated tip at 2 μm/s (A), and at 16 μm/s (B). (C-E) Domain size distribution for pentacene patterned, using a tip temperature of 500 ℃ and low contact force, at different scan speeds. (C) Pentacene patterns converted at scan speeds of 2 μm/s display the largest domains with a mean of 207 nm and a wide distribution of crystal sizes. (D) Pentacene patterns produced at a scan speed of 8 μm/s show both a higher mean and standard deviation. (E) Pentacene patterns grown at scan speed of 16 μm/s display a mean of about 100 nm and a low standard deviation. There is the faint appearance of alignment in the pentacene domains along the line of travel of the tip (left to right), as the heat transfer becomes more vertical in nature because of the small film thicknesses.

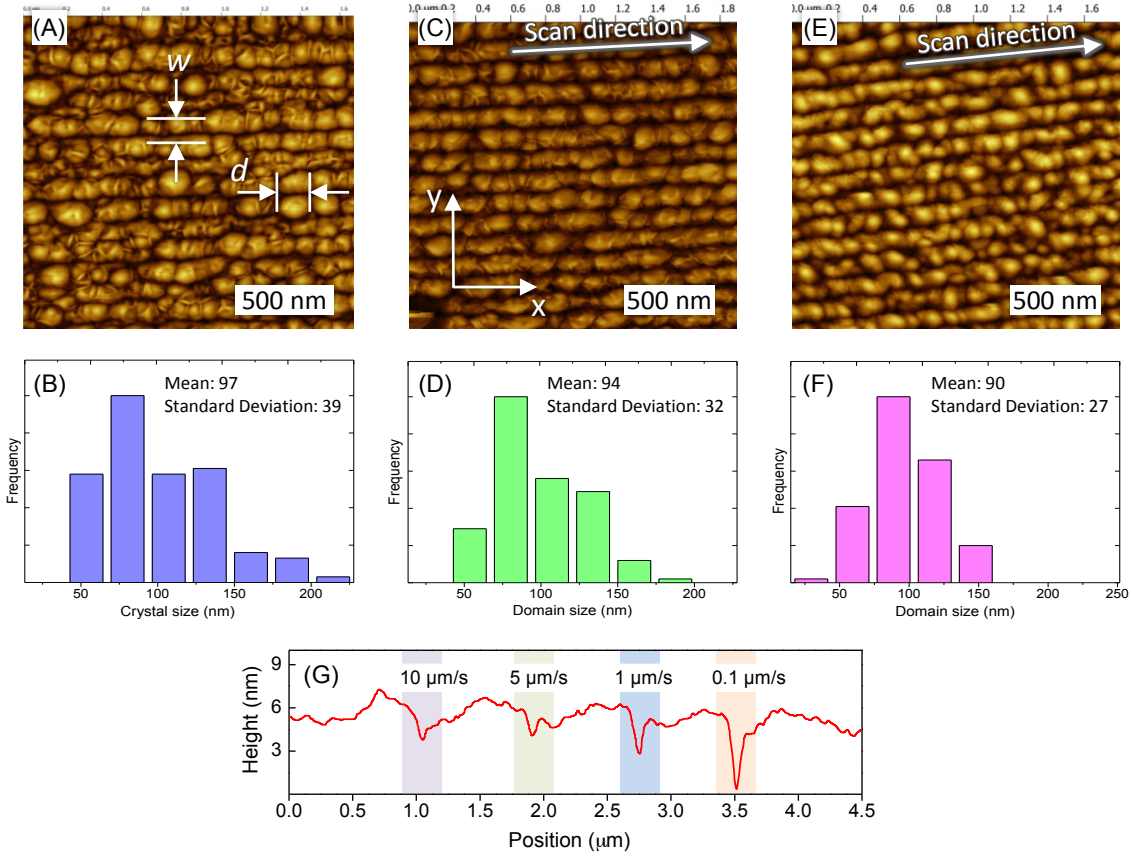

Figure 3. (A) AFM topography image of aligned pentacene nanoribbons-like structures 70-100 nm wide (*w*), oriented along the line of travel (from left to right) of the heated probe (500 ℃) produced at a speed of 8 μm s^{-1}. (B) Pentacene crystal domain size (*d*) distribution extracted from the AFM image in (A) showing a relatively large mean domain size and standard deviation. (C) AFM topography image of pentacene crystals oriented along the line of travel of the heated probe produced at a scan speed of 20 μm/s. (D) Pentacene crystal size distribution extracted from the AFM image in (C). (E) AFM topography image of pentacene nanoribbons-like structures oriented along the line of travel of the heated probe produced at a scan speed of **32** μm**/s.** (F) Pentacene domain size distribution extracted from the AFM image in (E) showing a smaller mean domain size and standard deviation. (G) Cross-section of an AFM image of four parallel lines of pentacene, converted at four different scan speeds, displaying successively deeper furrows for slower scan speeds due to increased degree of conversion of the pentacene precursor, but maintaining the 100 nm line width.

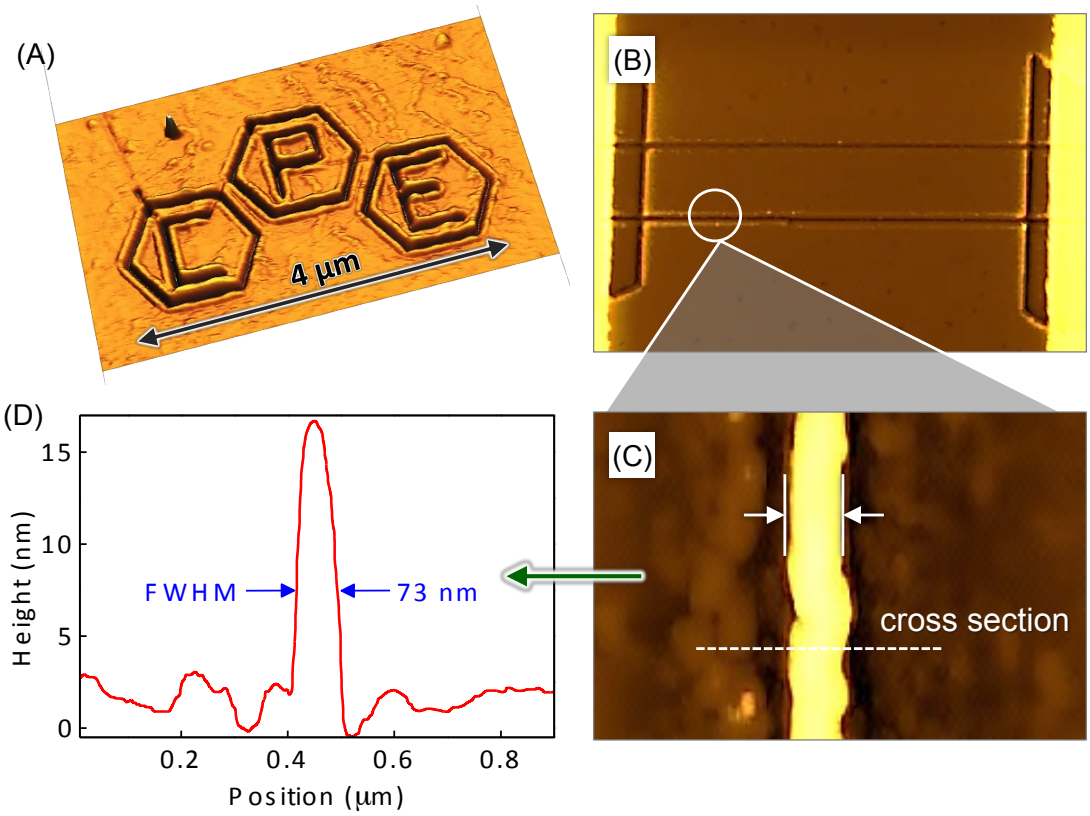

Figure 4. (A) AFM topography image of a micron-size logo of the Centre for Plastic Electronics (CPE) patterned by scanning thermal lithography onto a plastic substrate. (B) AFM topography image of pentacene nanoribbons drawn on pentacene precursor films between gold electrodes with a furrow width of ~100 nm. (C) AFM topography image of a stand-alone pentacene nanoribbon (patterned at a speed of 25 µm/s) after it has been developed in a methanol bath. (D) Cross-section of the pentacene nanoribbon in (C) revealing a nanoribbon width of ~73 nm calculated as the full width at half maximum (FWHM).

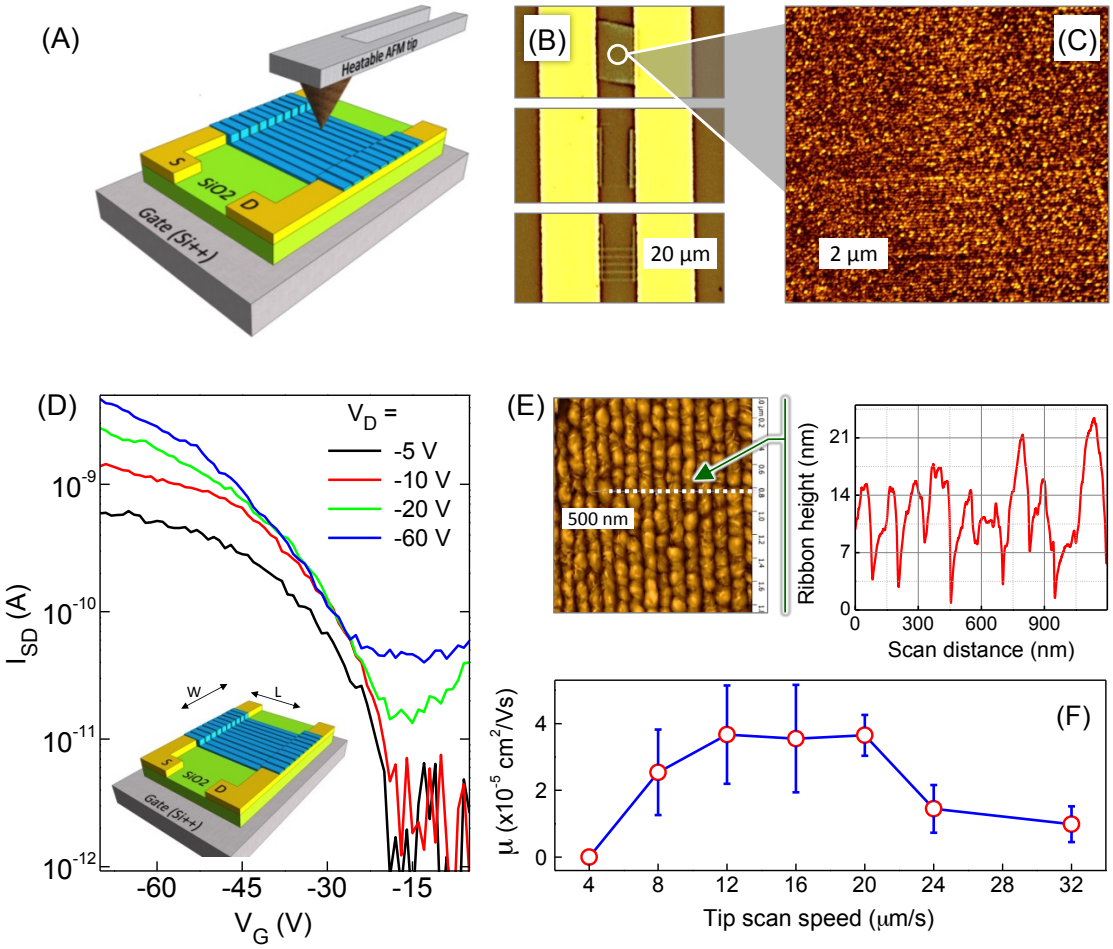

Figure 5. (A) Schematic representation of the pentacene transistor architecture and the heatable AFM tip used to pattern the pentacene precursor. (B) Optical microscopy image of semiconducting pentacene channels patterned over gold electrodes (bright regions) 10 µm (*L*) apart. (C) AFM topography image of densely packed pentacene nanoribbons 70-100 nm wide comprising the semiconducting block shown in B. (D) Transfer characteristics of a pentacene transistor, with the drain current plotted against varying gate voltage for different drain voltage levels, produced by scanning thermal lithography with a channel length of 2.5 µm and width of 7-8 µm. Inset: Schematic of the transistor structure used. (E) High-resolution AFM topography image of the pentacene nanoribbons contained in the actual transistor channel and the corresponding cross-section. (F) Graph displaying the relationship between hole mobility and thermal tip scan speed used to produce the transistors, with the associated error being the standard error on the mean.

The table of contents entry

Thermal scanning lithography is used to pattern semiconducting nanoribbon-like pentacene structures with ultra-high spatial resolution onto arbitrary substrates in air. The method allows control of pentacene crystal growth direction and domain size distribution. By combining these quasi 1-dimensional nanoribbon-like structures with conductive electrodes and a suitable gate dielectric, functional hole transporting (p-channel) transistors are demonstrated (Figure).

Keyword: Organic semiconductors, pentacene transistors, nanolithography, scanning thermal lithography, thermochemical lithography, scanning lithography

Authors: J. E. Shaw, P. N. Stavrinou and T. D. Anthopoulos*

Title: On-demand patterning of nano-structured pentacene transistors by scanning thermal lithography

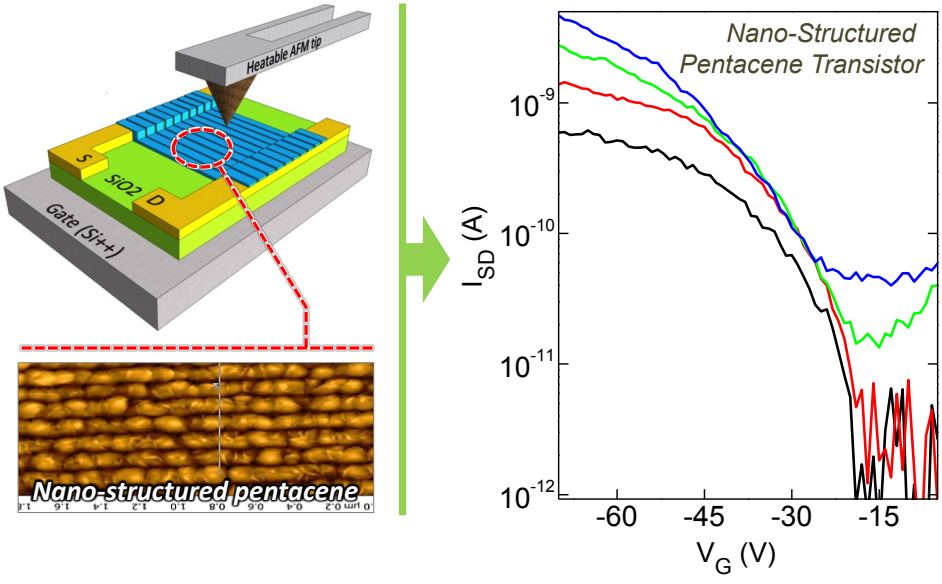

ToC Figure

References

1. T. W. Kelley, P. F. Baude, C. Gerlach, D. E. Ender, D. Muyres, M. A. Haase, D. E. Vogel,S. D. Theiss, *Chem Mater* **2004**. *16* 4413.
2. P. Lin,F. Yan, *Adv Mater* **2012**. *24* 34.
3. J. T. Mabeck,G. G. Malliaras, *Analytical and Bioanalytical Chemistry* **2006**. *384* 343.
4. L. Torsi, G. M. Farinola, F. Marinelli, M. C. Tanese, O. H. Omar, L. Valli, F. Babudri, F. Palmisano, P. G. Zambonin,F. Naso, *Nat Mater* **2008**. *7* 412.
5. U. Kunze, *Superlattice Microst* **2002**. *31* 3.
6. L. M. Demers, D. S. Ginger, S. J. Park, Z. Li, S. W. Chung,C. A. Mirkin, *Science* **2002**. *296* 1836.
7. S. Neubeck, F. Freitag, R. Yang,K. S. Novoselov, *Phys Status Solidi B* **2010**. *247* 2904.
8. D. Credgington, O. Fenwick, A. Charas, J. Morgado, K. Suhling,F. Cacialli, *Advanced Functional Materials* **2010**. *20* 2842.
9. O. Fenwick, L. Bozec, D. Credgington, A. Hammiche, G. M. Lazzerini, Y. R. Silberberg,F. Cacialli, *Nat Nanotechnol* **2009**. *4* 664.
10. H. J. Mamin, *Appl Phys Lett* **1996**. *69* 433.
11. H. J. Mamin,D. Rugar, *Appl Phys Lett* **1992**. *61* 1003.
12. K. L. Grosse, M. H. Bae, F. F. Lian, E. Pop,W. P. King, *Nat Nanotechnol* **2011**. *6* 287.
13. K. Park, G. L. W. Cross, Z. M. M. Zhang,W. P. King, *J Heat Trans-T Asme* **2008**. *130*.
14. J. Lee, T. Beechem, T. L. Wright, B. A. Nelson, S. Graham,W. P. King, *J Microelectromech S* **2006**. *15* 1644.
15. D. B. Wang, R. Szoszkiewicz, M. Lucas, E. Riedo, T. Okada, S. C. Jones, S. R. Marder, J. Lee,W. P. King, *Appl Phys Lett* **2007**. *91*.
16. Z. Q. Wei, D. B. Wang, S. Kim, S. Y. Kim, Y. K. Hu, M. K. Yakes, A. R. Laracuente, Z. T. Dai, S. R. Marder, C. Berger, W. P. King, W. A. de Heer, P. E. Sheehan,E. Riedo, *Science* **2010**. *328* 1373.
17. S. Kim, Y. Bastani, H. D. Lu, W. P. King, S. Marder, K. H. Sandhage, A. Gruverman, E. Riedo,N. Bassiri-Gharb, *Adv Mater* **2011**. *23* 3786.
18. J. Duvigneau, H. Schonherr,G. J. Vancso, *Acs Nano* **2010**. *4* 6932.
19. J. Duvigneau, H. Schonherr,G. J. Vancso, *Langmuir* **2008**. *24* 10825.
20. J. Duvigneau, H. Schonherr,G. J. Vancso, *Acs Applied Materials & Interfaces* **2011**. *3* 3855.
21. D. Pires, J. L. Hedrick, A. De Silva, J. Frommer, B. Gotsmann, H. Wolf, M. Despont, U. Duerig,A. W. Knoll, *Science* **2010**. *328* 732.
22. U. T. D. M. Despont, J. E. Frommer, B. W. Gotsmann, J. L. Hedrick, C. J. Hawker, R. D. Miller, Scanning Probe-Based Lithography Method, 20110020533, **2011.**
23. A. Afzali, C. D. Dimitrakopoulos,T. L. Breen, *J Am Chem Soc* **2002**. *124* 8812.
24. A. S. Basu, S. McNamara,Y. B. Gianchandani, *J Vac Sci Technol B* **2004**. *22* 3217.
25. V. Ignatescu, J. C. M. Hsu, A. C. Mayer, J. M. Blakely,G. G. Malliaras, *Appl Phys Lett* **2006**. *89*.
26. R. Ruiz, D. Choudhary, B. Nickel, T. Toccoli, K. C. Chang, A. C. Mayer, P. Clancy, J. M. Blakely, R. L. Headrick, S. Iannotta,G. G. Malliaras, *Chem Mater* **2004**. *16* 4497.
27. P. T. Herwig,K. Mullen, *Adv Mater* **1999**. *11* 480.
28. G. H. Gelinck, H. E. A. Huitema, E. Van Veenendaal, E. Cantatore, L. Schrijnemakers, J. B. P. H. Van der Putten, T. C. T. Geuns, M. Beenhakkers, J. B. Giesbers, B. H. Huisman, E. J. Meijer, E. M. Benito, F. J. Touwslager, A. W. Marsman, B. J. E. Van Rens,D. M. De Leeuw, *Nat Mater* **2004**. *3* 106.
29. G. Horowitz, *Adv Mater* **1998**. *10* 365.

Supplementary Information

On-demand patterning of nano-structured pentacene transistors by scanning thermal lithography

By *Joseph E. Shaw, Paul N. Stavrinou* and *Thomas D. Anthopoulos*

1 Imaging of converted pentacene structures

In this section we discuss further images of converted pentacene features, obtained by atomic force microscopy (AFM) and by conventional light and polarised light microscopy.

1.1 Atomic force microscopy (AFM) measurements

All AFM topography images used in the manuscript were not deconvoluted, as there was hardly any discernible difference between the deconvoluted image and the original image. This is illustrated in **Figure S1** and is valid for all relevant figures in the manuscript. The deconvolution process was completed using Gwyddion AFM data analysis software and involved reconstruction of the probe with the Blind Tip Estimation option, followed by production of the deconvoluted image with the Surface Reconstruction option. The minimum impact of the tip convolution was also observed for as-spun precursor films and hot-plate converted pentacene films shown in **Figure 1(c-d).**

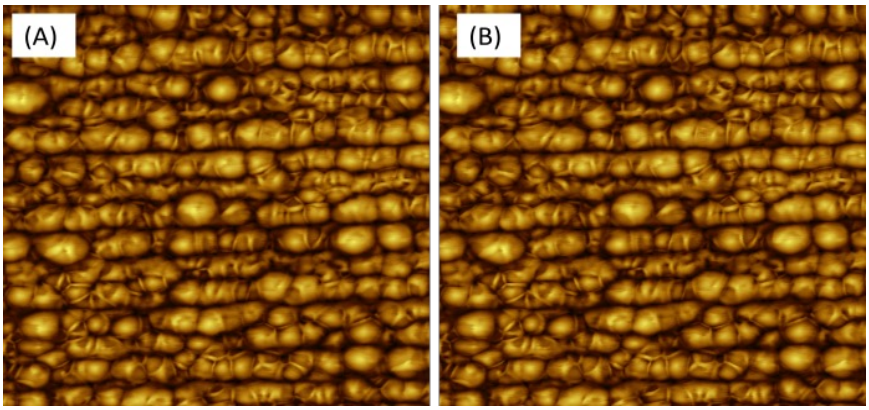

Figure S1*: Comparison demonstrating the almost entire absence of difference between the deconvoluted AFM topography image shown in (A), and the original topography image (i.e. as-measured) shown in (B).*

1.2 Polarized light optical microscopy measurements

Patterned pentacene structures of resolvable size were also imaged using conventional optical microscopy and polarised light microscopy. Crossed polariser optical images were taken in the second case in order to assess the crystalline nature of the converted features through the observation of optical birefringence. A representative optical microscopy image of arbitrary shaped converted pentacene structures is shown in **Figure S2** where the structures, patterned between a 10 μm channel gap between gold source and drain electrodes [**Figure S2(a)**], are visible and appear as the pale blue. The patterned areas are found to be crystalline in nature as evident by the strong optical birefringence [**Figures S2(b-c)**] seen through cross-polarizers. In contrast, the film areas covered by the amorphous precursor appear black.

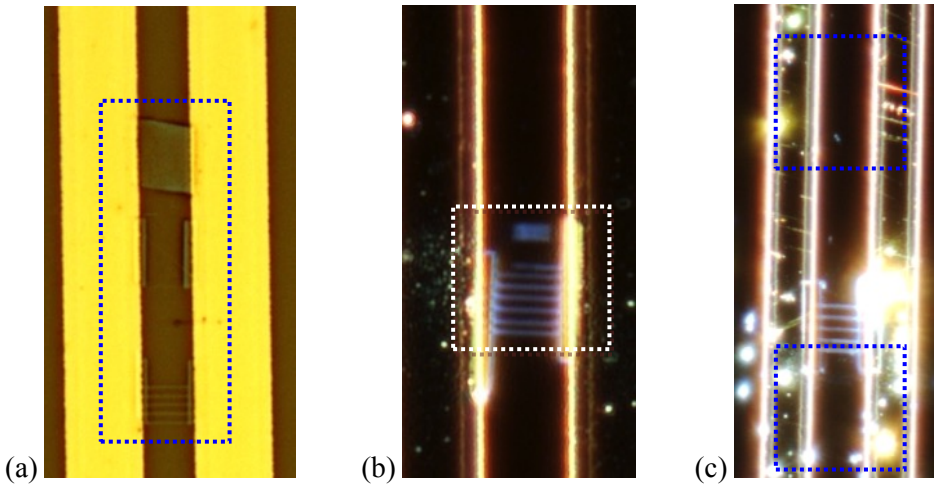

Figure S2*: (a) conventional light microscopy image showing the converted pentacene features (blue areas) patterned between two gold electrodes (bright areas). The remaining area shows the unconverted precursor surrounding the patterned features. (b) & (c) polarised light*

microscopy images of patterned pentacene ribbons and blocks drawn between gold electrodes spaced 10 µm apart, showing the features as blue due to the birefringence caused by the pentacene crystals. Dark/black areas in the image represent the amorphous uncovered precursor film (i.e. no birefringence due to the amorphous nature of the precursor film).

2 Effects governing the production of pentacene features by scanning thermal lithography

In order to successfully control the patterning of the pentacene precursor, a thorough analysis of all the different parameters affecting its conversion into pentacene was undertaken; with special attention paid to the factors affecting the minimum width of patterned pentacene features. It is well established that the heat transfer dynamics of a tip are different to those of a bulk-heating hotplate. In the latter case the critical parameter is temperature while in the case of scanning thermal lithography, a combination of parameters has to be optimised in order to convert the precursor and produce features of a desired width and depth. The three important parameters (for a given tip width and material/substrate combination) are the scan speed of the tip, tip temperature and contact force. The film thickness also has an important role as it governs the maximum width and depth of the converted feature. Next the different parameters are discussed in detail.

2.1 Tip temperature and scan speed

The two parameters having the greatest degree of influence on the temperature experienced by the precursor are the tip scan speed and tip temperature. The variation of tip temperature would directly affect the experienced temperature. In terms of variation of scan speed, a faster scan speed means shorter duration of contact for a given area of precursor with the heated tip and so less heat energy is transferred and a lower temperature is experienced by the precursor. An analogy to this is waving a hand through a candle flame of fixed temperature; waving it through

at high speed results in a feeling of warmth, whereas passing your hand through very slowly will result in your hand being burnt. So in order for the material to experience the optimal precursor conversion temperature, we need to have a balanced combination of tip temperature and scan speed; a low tip temperature will require a slow scan speed in order for the precursor to be converted, as opposed to higher tip temperatures, where the scan speed is increased, in order for the precursor to still experience the same conversion temperature. The tip temperature of 500 °C was chosen as it was the maximum tip temperature possible and would result in conversion of the precursor at faster scan speeds and hence to an improved device production rate. To avoid chemical decomposition and/or sublimation of the material due to high tip temperature, the speed of the tip at which conversion occurred was carefully optimised. This was achieved by monitoring the conversion of the precursor to pentacene crystals through the use of polarised light microscopy and by evaluating the electrical characteristics of the converted pentacene structures using transistor measurements. Based on these measurements it was found that the optimal conversion speed, for a fixed tip temperature of 500 °C, was between 12-20 μm/s [**Figure 5(F)**]. For higher tip speed (i.e. resulting in an increase temperature experienced by the precursor film) the precursor material was found to sublime while for lower speeds the precursor remained largely unconverted.

Variation in scan speed and tip temperature has the secondary effect of varying the width/depth of the features. When a heat source is in contact with a material, there is a temperature gradient, originating from the heat source, with decreasing temperature contours emanating from the source, with the width and depth of a converted pentacene feature being the width and depth of the precursor volume with a temperature ≥ precursor conversion temperature. For a heat source of a higher temperature, the conversion depth and width would be greater; with modification of the heat source "temperature" (temperature experienced at the tip/precursor interface) achieved by increasing or decreasing the scan speed and/or tip temperature.

2.2 Effect of film thickness

Film thickness also has an influence on the width/depth of the resulting features (as was demonstrated by Fenwick et al and our own simulations), with a thinner film resulting in shallower/thinner features. As the film thickness decreases below the tip contact width, the heat transfer becomes increasingly vertical, with a feature resolution limit being approximately the tip contact width. To this end, it was decided to use the thinnest film possible film thickness that was physically and electrically continuous in order to produce the thinnest features we could.

2.3 Effect of contact force

There is controversy over whether the contact force actually affects the interface temperature. FEA simulations by Nelson *et al*[1] say that higher contact forces result in an increase of the contact area of the tip due to the tip being pushed deeper into the polymer layer. These simulation results are in contrast to experimental evidence of thermal lithography on polymers where the material softening temperatures were found to be independent of the force applied to the tip[2], this may have been due to the need for heat to diffuse into the material around the tip before motion into the substrate was detectable[3]. The variation of contact force could increase and decrease the width and depth of features; in an organic (mechanically soft) material, an increase in contact force has the effect of pushing the thermal tip further into the polymer film, thus increasing the contact area of the tip with the film and the conversion temp is experienced to a greater depth and width. In order to simplify matters and in deference to the fact that we could exert little control of the contact force we kept the contact force variation to two settings, low contact force (just at the point of contact of the tip on the surface) and high contact force (6 V bias).

2.4 Substrate properties

Aside from parameters directly involved with the tip, there are other factors which could affect the heat transfer from the tip; thermal properties of the material and the thermal properties of the underlying substrate. The underlying substrate can have large effects on thermal heat transfer, as researched by Nelson et al[1], and more recently by Tolk et al[4]. In order for a material to reach a certain critical temperature, the material deposited on a substrate with a high thermal conductivity requires a tip temperature higher than material on a substrate of low thermal conductivity. This is due to the substrate below the material absorbing heat through the material itself. The effects can be quite profound in terms of the temperature needed for the scanning probe tip to convert precursors, but an increase in substrate thermal conductivity has limited effects on the feature resolution[4]. This has to be born in mind when the substrate is chosen; the substrate we used was 300 nm of SiO_2 on silicon, which also doubled up as the transistor dielectric layer and coincidentally a material with a low thermal conductivity.

3 Computer simulation

3.1 Scanning thermal lithography finite element simulations

Simulations of both a stationary and a moving tip were performed using the Heat Transfer Module of Comsol Multiphysics 4.0 finite element simulation software. These simulations were undertaken in order to provide some estimates of theoretical performance and optimal settings of the scanning thermal lithography experimental set-up. The simulations were divided into two parts: 1) steady-state heat transfer of a stationary heated tip and 2) transient heat transfer of a heated tip moving at pre-set velocities and whilst stationary. These simulations allow the modelling of the depth and width of the features produced by varying tip temperatures and velocities.

3.2 Model basis and theory

The simulations were set up and run in two dimensions. The basic components of each model were a substrate of silicon dioxide on which was deposited a layer of polymer precursor whose thickness was varied in the simulations. In exploratory simulations, the heated tip was represented by an area roughly corresponding to the tip's geometrical footprint on the polymer surface, which was heated to a desired temperature to act as the heat source. Both the silicon dioxide substrate and the polymer layer were modelled as or semi-infinite planes (length is several orders of magnitude greater than width); the surface layer and sides of the polymer had thermally insulating properties whilst the silicon dioxide substrate bottom and sides were connected to a heat source of 20 °C to simulate ambient conditions[5]. A diagram for this basic model setup is shown in **Figure S3**.

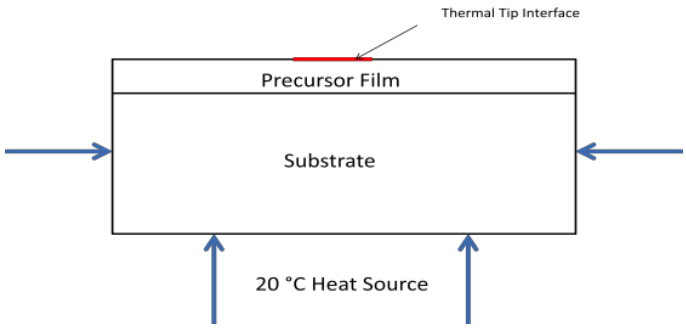

Figure S3*: Schematic of the model basis for Comsol Multiphysics simulations. The basis comprises of a precursor film on top of a substrate. The substrate bottom and sides were connected to a heat source of 20 °C to simulate room temperature ambient conditions. The interface with the heatable AFM tip is represented by a heat source of a fixed temperature.*

Although there is radiative heat transfer between the heat source and the material previous simulations[5], highlight the negligible effect this radiative heat transfer has, and so based on these considerations, it was decided to omit radiative heat transfer from the simulations and thus this model deals solely with conductive heat transfer between materials. Since the quantity of interest is the temperature of the polymer, and the temperature at the interface created by the

resistive heating was determined by calibration, it is not necessary to create an accurate representation of the silicon heating tip. This greatly simplifies the simulation model and allows the tip to be modelled as a boundary on the surface of the polymer of the same size as the tip footprint which is heated to the desired temperature; conduction allows the heat to spread through the material layer.

The variable parameters affecting the amount of heat transferred from the tip to the material are the temperature of the tip and the speed at which the tip is moved over the surface of the material; the material must have enough heat to reach its conversion temperature. In the case of polymer precursor layers, the material has to be converted for its full depth, so that the converted features are anchored to the substrate and are not removed during the development step[5]. The substrate material used in these simulations was SiO_2 which means a thermal conductivity (k) of 1.3 W mK^{-1}, a heat capacity (C_p) of 820 J kg^{-1} K^{-1} and a density (ρ) of 2600 kg m^{-3}. Since material studies of the pentacene precursor could not be made, it was decided to run simulations on two different material types, on one end of the scale, crystalline pentacene; k = 0.58 W mK^{-1}, C_p = 311 J kg^{-1} K^{-1} and ρ = 1300 kg m^{-3}, and on the other end a polymer, PMMA; k = 0.19 W mK^{-1}, C_p = 1420 J kg^{-1} K^{-1} and ρ = 1190 kg m^{-3}. In our opinion, using simulations with material properties very close to those of the precursor are not of the greatest importance. These simulations are not meant to be very accurate representations or predictions of the results of the actual scanning thermal lithography attempts, but are merely used to identify trends and relationships between various parameters of temperature, film thickness and scan speed.

3.3 Steady state simulations

The material used in this project is a solution processible pentacene precursor. The latter was spin coated onto substrates and then converted into pentacene through the application of

heat through the heatable AFM tip. To remove excess precursor that has not been converted to pentacene, the substrate would have to be washed in a solvent development step with methanol. However, to ensure the structural integrity of the converted features following this development step, the conversion of the precursor has to be completed throughout the thickness of the sample i.e. all the way to the interface with the substrate. In order to achieve this, a temperature has to be reached at substrate level that is sufficient for conversion to occur. A steady state simulation can be used to model a stationary tip in contact with a polymer layer on a substrate, and once simple material parameters are entered (e.g. thermal conductivity, density and heat capacity), temperature profiles can be modelled.

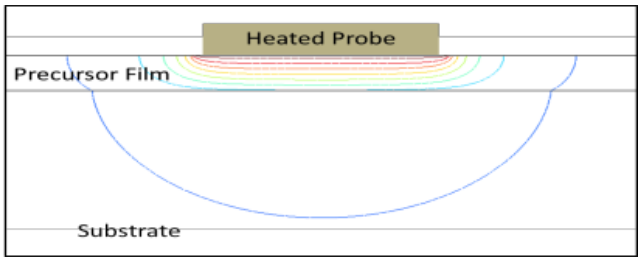

Figure S4*: Diagram displaying 20 nm thin polymer film, on top of a silicon dioxide substrate, in contact with a 100 nm wide heat source of constant temperature, with the accompanying contours of constant temperature.*

When a 100 nm wide contact boundary is used, the temperature contours within the polymer film as shown in **Figure S4** are obtained. Using a definition of feature width as the width of the contour which touches the substrate below the polymer layer[5], simulations were run where the film thickness was varied in order to observe the effects this would have on overall feature width for both pentacene and PMMA. The calculated results for both materials are displayed in **Figure S5**.

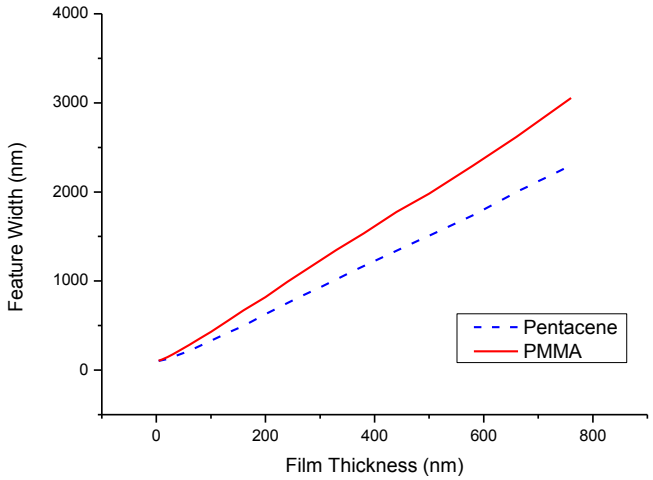

***Figure S5**: Graph of the feature width resulting from differing film thickness for PMMA and pentacene, demonstrating an approximately linear increase of feature width with film thickness.*

It is clear from this figure, that an increased film thickness increases the minimal width of the converted feature for both materials, this reinforces the concept that higher resolution of feature size (e.g. for making the thinnest nanowires) could be achieved by reducing the thickness of the films as much as possible. The simulations also prove the concept[4] that in the case where the contact width of the tip greatly exceeds the film thickness, the feature width reaches a minimum roughly corresponding to the contact width of the heated probe tip. The difference between the material performances is due to the higher thermal conductivity and the lower heat capacity (the amount of energy needed to raise an amount of material by a fixed temperature) of the pentacene material as compared to the PMMA material which results in wider features for the pentacene material than for PMMA for a given film thickness.

3.4 Transient analysis

For the more complicated case of a moving heated tip, the footprint representing the tip was moved along the surface, taking advantage of the transient motion capabilities of the Comsol software that allows variation of the tip speed. Simulations of a transient nature were used to

model variation of experienced temperature within the polymer for varying speed (**Figure S6**), as well as the maximum speed for varying film thickness that full precursor conversion occurs (at 120 °C) to the base of the material.

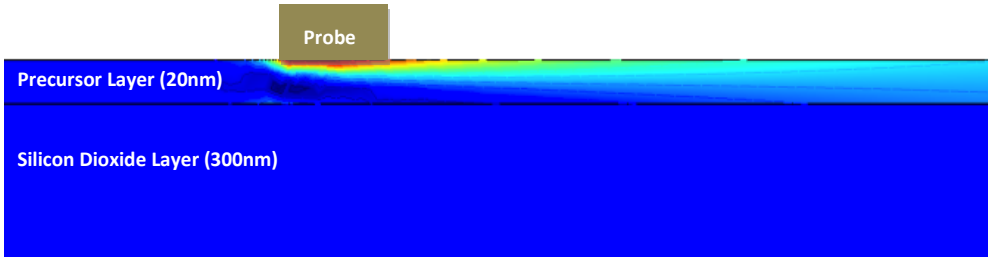

***Figure S6**: Schematic displaying a heated tip travelling across the surface of the precursor. The contours and colour grades represent changing temperatures ranging from higher temperatures at the red end and lower temperatures at the dark blue end.*

The results of the transient analysis reinforced the idea that a faster tip movement would lead to a lower temperature experienced by the precursor. Simulations of a 20 nm thick precursor film on top of a silicon dioxide substrate using a heated tip with a 500 ℃ interface temperature, where the interface diameter was 100 nm (identical to the setup used for actual tip experiments), showed that the conversion temperature of 120 ℃ was not achieved at the interface for tip speeds above 1.16 μm s^{-1} for PMMA and 13.3 μm s^{-1} for pentacene. Once again, the difference in performance of the materials is due to the higher thermal conductivity and the lower heat capacity (the amount of energy needed to raise an amount of material by a fixed temperature) of the pentacene material in contrast to the PMMA material; this yields the expected result that the tip can scan at far higher speeds at all temperatures with the pentacene material.

The results for the secondary simulations to record the maximum scan speed at which the conversion temperature was achieved at the substrate and polymer interface are displayed in **Figure S7**. These graphs display an almost exponential increase in speed as the film thickness decreases, highlighting the dramatic increase in the speed efficiency of pentacene conversion that

can be achieved by decreasing film thickness to a minimum. All these simulations indicate measures that one can take to maximize the resolution (decreasing the feature width to its minimum) and conversion efficiency, by decreasing the film thickness and increasing the tip temperature as much as is possible, allowing us to greatly increase the scan speed.

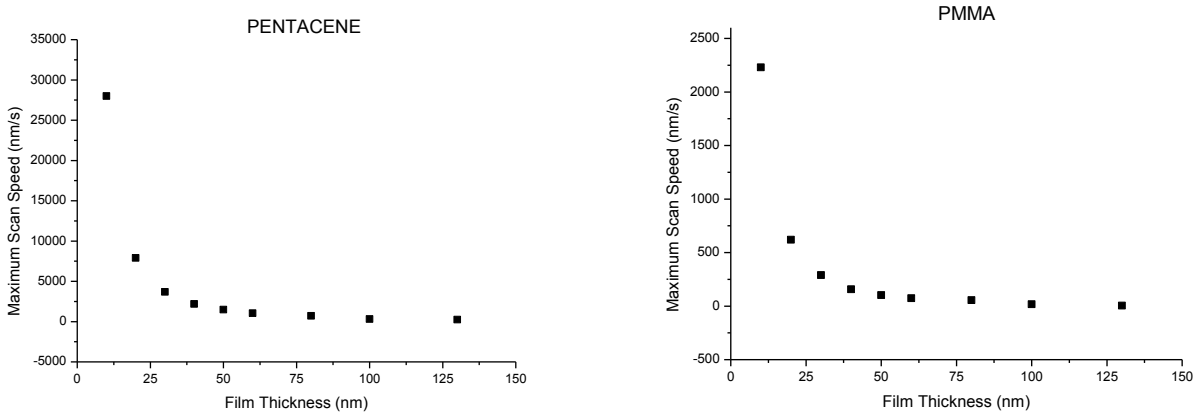

Figure S7*: Graphs of the maximum scan speed possible for variation in film thickness, displaying the nearly exponential increase in scan speed for decreasing film thickness for both pentacene (left) and PMMA (right).*

References for SI section

1. B. A. Nelson,W. P. King, *Nanosc Microsc Therm* **2008**. *12* 98.
2. B. A. Nelson,W. P. King, *Rev Sci Instrum* **2007**. *78*.
3. W. P. King,K. E. Goodson, *J Heat Trans-T Asme* **2007**. *129* 1600.
4. M. Tolk, O. Fenwick, S. Ahmad,F. Cacialli, *J Appl Phys* **2012**. *111*.
5. O. Fenwick, L. Bozec, D. Credgington, A. Hammiche, G. M. Lazzerini, Y. R. Silberberg,F. Cacialli, *Nature Nanotechnology* **2009**. *4* 664.